IEEE Access
Multidisciplinary ⁝ Rapid Review ⁝ Open Access Journal

Received 11 August 2025, accepted 24 August 2025, date of publication 2 September 2025, date of current version 9 September 2025.

Digital Object Identifier 10.1109/ACCESS.2025.3605534

RESEARCH ARTICLE

Scale-Free and Phase-Agnostic Detection of Interturn Short-Circuit Faults in Permanent Magnet Synchronous Motors

MIKYUNG HWANG, JONGHYEOK KIM, HYUNTAK LEE, AND HYUNSEOK OH
Department of Mechanical and Robotics Engineering, Gwangju Institute of Science and Technology, Gwangju 61005, Republic of Korea

Corresponding author: Hyunseok Oh (hsoh@gist.ac.kr)

This work was supported by the National Research Foundation of Korea (NRF) grant funded by the Korea Government [Ministry of Science and ICT (MSIT)] (No. RS-2025-00517566, No. RS-2022-00144441). This work was supported by Korea Institute for Advancement of Technology (KIAT) grant funded by the Korea Government [Ministry of Trade, Industry and Energy (MOTIE)] (RS-2025-02263945, Human Resources Development (HRD) Program for Industrial Innovation).

ABSTRACT This study presents a scale-free and phase-agnostic method for detecting interturn short-circuit faults (ISCFs) in the stator windings of permanent magnet synchronous motors (PMSMs). The proposed method integrates denoising and feature extraction with a crest-factor-based health indicator. A wavelet-based denoising method with average peak extraction is devised to enhance the sensitivity to fault-induced current deviations while suppressing external noise. The crest factor is modified to enable phase-agnostic detection across stator windings. To eliminate scale dependency associated with motor capacity, the modified crest factor is further calibrated using baseline data obtained under healthy conditions. The resulting health indicator, namely max-min crest factor, enables consistent and reliable ISCF detection without requiring motor-specific parameters or prior knowledge of the faulty phase. The effectiveness of the proposed method is validated through multiple case studies, including 1) numerical simulations, 2) laboratory-scale testbed experiments on small-capacity PMSMs (100 W and 1 kW), and 3) full-scale testing on an 82.5 kW PMSM under realistic operating conditions. The experimental results demonstrate that the method reliably detects ISCFs regardless of fault location or motor scale.

INDEX TERMS Health indicator, interturn short-circuit fault, motor current signature analysis, permanent magnet synchronous motor.

I. INTRODUCTION

In manufacturing lines such as petrochemical plants, steel mills, and thermal power plants, permanent magnet synchronous motors (PMSMs) of various capacities are used. The malfunction of even a single motor in such environments can result in the shutdown of an entire production line, leading to significant financial losses. For instance, a 30-minute interruption in an automotive assembly line has been reported to cause losses of approximately one million US dollars.

Interturn short-circuit faults (ISCFs) occurring in stator windings are considered particularly critical among the dominant failure modes in PMSMs [1]. The faults can lead to localized overheating and eventually develop into turn-to-turn faults [2]. Progression of such faults can further lead to phase-to-phase or ground faults [3]. In severe cases, thermal damage can result in irreversible demagnetization of the rotor's permanent magnets. Therefore, the detection of ISCFs at the initial stage of insulation degradation is essential to prevent further damage.

The methods for detecting ISCFs can be grouped into model-based, data-driven, and signal-processing-based. First, model-based approaches use mathematical models that simulate the behavior of the physical system of interest. When measurements from the real system differ from the values of the mathematical model, a fault is considered to have been detected [4], [5], [6], [7], [8]. Second, data-driven approaches use pattern relationships extracted from data to make decisions and perform predictions. The approaches are particularly effective when large amounts of data are

The associate editor coordinating the review of this manuscript and approving it for publication was Zhuang Xu.

available from the system [9], [10], [11], [12]. Last, signal-processing-based approaches detect faults by analyzing signals associated with faults. For example, high-frequency current injection analysis [13] and current residual-based analysis [14] were developed to extract useful features from stator currents. In addition, Park's vector analysis [15] has been applied to detect asymmetries and fault-related harmonics in three-phase synchronous motors. Recently, Wu et al. [16] analyzed ISCFs in PMSMs by monitoring speed, current, and zero-sequence voltage. Experimental verification showed that detection performance varied significantly depending on operating conditions, although the fault indicator increased with fault severity.

This paper proposes a scale-free and phase-agnostic method for detecting ISCFs in PMSMs. The proposed method is motivated by the observation that stator current signals from PMSMs of different capacities exhibit similar waveform characteristics. Among various signal descriptors, the crest factor was selected for its sensitivity to impulsive components induced by ISCFs. In this study, the original crest factor is modified to ensure stator phase-agnostic detection. Furthermore, the modified crest factor (MCF) is calibrated to enable scale-free detection. The proposed method is validated through multiple case studies. The contribution of this paper can be summarized into threefold. First, a scale-free health indicator, namely max-min crest factor (MMCF), is developed that maintains consistent ISCF detection performance across PMSMs of different capacities without requiring motor-specific parameters. Second, a phase-agnostic detection approach is proposed that integrates information from all three-phase current signals simultaneously, enabling fault detection regardless of the faulty phase location. Last, the method requires only standard current measurements without additional sensors or motor-specific parameters, facilitating implementation in industrial environments.

The remainder of this paper is organized as follows. Section II presents a literature review on ISCF detection methods and identifies the challenges of achieving scale-free and phase-agnostic fault detection across different motor capacities. Section III presents a novel health indicator for scale-free and phase-agnostic ISCF detection that integrates wavelet-based denoising, MCF calculation, and capacity-independent calibration. To verify the effectiveness of the proposed method, Section IV describes three case studies using ISCF simulations and testbeds with artificially injected faults. Section V concludes the paper with a discussion of future research.

II. LITERATURE REVIEW

The theoretical foundation needed to understand the detection of ISCFs in PMSMs is reviewed from three main aspects: the failure mechanism of ISCFs, existing fault detection methods focusing on capacity dependency issues, and signal analysis techniques applicable to fault detection. This review identifies the need for scale-free and phase-agnostic fault detection methods and explains the challenges.

A. ISCF IN PMSMS

The failure mechanism analysis of ISCFs occurring in stator windings shows the progression of insulation degradation. The degradation of the insulation material surrounding the winding coils progresses, starting with micro-cracks or partial discharges that weaken the electrical and mechanical properties of the insulation [17]. This degradation can be confirmed by a decrease in insulation resistance values, which drop from several mega-ohms (MΩ) in the normal state to tens of kilo-ohms (kΩ) as degradation progresses, eventually reaching a complete short-circuit state.

Motor performance deteriorates at an exponential rate with increasing severity of ISCFs. As a physical result of this fault, the current waveform deviates from the nominal form to include irregular peaks or harmonic components. These waveform distortions are small and intermittent, necessitating sensitive fault detection indicators that use the statistical characteristics of the waveform. When ISCFs progress, an additional current flowing through the short-circuit resistance is generated in the shorted part. This short-circuit current affects the normal operating current of the motor. It should be noted that it affects the current waveform not only in the phase where the short-circuit occurred but also in other phases [18]. These combined effects can appear differently depending on the motor's capacity and load conditions at the early stage of the fault, further emphasizing the importance of scale-free and phase-agnostic fault detection methods.

B. SCALE-FREE AND PHASE-AGNOSTIC DETECTION FOR ISCFS

Model-based approaches rely on mathematical representations of the motor's electromagnetic behavior, typically employing equivalent circuit models or finite element analysis. While theoretically sound, the methods require precise knowledge of motor-specific parameters including winding inductances, resistances, and magnetic flux distributions [7]. The challenge arises from the nonlinear relationship between these parameters and operating conditions—magnetic saturation alters inductances, while temperature variations affect resistances according to material-specific thermal coefficients [18]. In industrial settings with thousands of motors from various manufacturers, the practical impossibility of characterizing these nonlinear parameter variations undermines the theoretical foundations of model-based fault detection.

Data-driven approaches attempt to circumvent parameter dependency by learning fault patterns directly from operational data. However, these methods face theoretical limitations rooted in statistical learning theory and practical implementation challenges. Data-driven approaches for ISCF detection face practical limitations due to their high computational costs, including extensive data training requirements, large model sizes, and substantial computational resources [19]. The fundamental challenges lie in the frequency of ISCF occurrence, which is only about 1%, resulting in a severe class imbalance that violates the independent and identically distributed assumption underlying most machine learning algorithms [20], [21]. Furthermore, the high dimensionality of motor operating conditions combined with limited fault samples results in poor generalization across different motor capacities [22], [23].

To address the limitations of model-based and data-driven approaches, recent research has focused on signal-processing-based approaches that use health indicators for fault detection, offering lower computational overhead while maintaining fault detection effectiveness [24]. However, their effectiveness depends on the signal-to-noise ratio and the spectral characteristics of fault indicators since they extract fault signatures from measured signals. The fundamental challenge lies in the scale-dependent relationship between fault signatures and motor parameters. The same physical fault severity produces different electrical manifestations depending on motor impedances, which scale nonlinearly with motor capacity [25]. This scaling effect particularly impacts harmonic analysis in low-speed operations, where mechanical dynamics couple with electrical phenomena to mask fault signatures [16]. Moreover, existing health indicators suffer from a critical limitation: they are not scale-free, meaning their baseline values vary across different motor capacities and configurations.

The need for scale-free and phase-agnostic motor fault detection is becoming increasingly important in industrial settings. Even with the same fault severity (e.g., the same short-circuit ratio), the electrical characteristics of faults can vary significantly depending on motor capacity and structure [25]. This demonstrates the fundamental limitation that existing fault detection methods have been primarily optimized for single-capacity motors, making it difficult to provide consistent performance in industrial environments where motors of various capacities coexist. To address this problem, it is urgent to develop scale-free and phase-agnostic fault detection methods to identify and normalize fault patterns common to motors of different capacities.

C. SIGNAL PROCESSING-BASED DETECTION FOR ISCFS

To overcome the limitations of existing fault detection methods, it is required to develop signal-processing-based approaches applicable to motors of various capacities. Motor current signal signature analysis (MCSA) is effective due to its advantages of requiring no additional sensors and being non-invasive [26]. MCSA is based on the principle that ISCFs cause distortions in the electromagnetic field distribution, leading to detectable asymmetries in the stator current waveforms. The MCSA techniques can be divided into time, frequency, and time-frequency domain analysis.

Time domain analysis extracts fault signatures directly from current waveforms without frequency transformation. Parvin et al. [27] proposed a transformer neural network approach using stator α-β currents that achieved over 96% accuracy in estimating both shorted turns and fault current amplitude. Jeong et al. [28] developed an early-stage fault detection method using negative-sequence components through symmetrical component analysis, where fault conditions increase negative-sequence levels due to stator winding imbalance.

Frequency domain analysis identifies fault signatures through spectral characteristics of current signals. Romeral et al. [29] demonstrated that ISCFs cause significant increases in the 3rd, 5th, and 7th harmonic components of the fundamental frequency, providing clear spectral fault indicators. Cruz and Cardoso [15] developed the extended Park's vector approach (EPVA), which detects $2f_s$ components (twice the fundamental frequency) in the Park's vector modulus spectrum that appear when ISCFs create stator winding asymmetries.

Time-frequency domain analysis combines temporal and spectral information to capture non-stationary fault characteristics. Zhao et al. [30] proposed adaptive feature mode decomposition (AFMD) with multiscale complex component current trajectory analysis. However, this approach suffers from a large computational burden and limited validation scenarios.

Among these various analysis methods, time domain analysis has the advantage of low computational complexity and suitability for real-time fault detection in industrial environments. Within the framework of statistical signal processing, the crest factor serves as a fundamental morphological descriptor that quantifies signal impulsiveness through the mathematical ratio of peak amplitude to root-mean-square (RMS) value. The crest factor is defined as the peak value of the waveform divided by the root mean square value of the waveform. For an ideal sine wave, the crest factor is 1.414, and it increases when the waveform includes impulses or abnormal peaks. The crest factor can effectively distinguish between impulses and random signals that are difficult to differentiate by frequency analysis. It can also detect faults without prior knowledge of fault-related frequencies, making it universally applicable to various types of faults. With these characteristics, the crest factor is also widely used in bearing and gearbox fault detection [31], [32], [33].

The crest factor has limitations. First, it is sensitive to noise and appears differently depending on motor capacity. Electromagnetic interference or switching noise in industrial environments degrades the accuracy of crest factor calculation [34]. Also, even in the same fault state, waveform characteristics differ depending on motor capacity and winding structure, making it challenging to apply a single reference value to motors of different capacities. To overcome these limitations, previous studies have applied signal preprocessing techniques such as wavelet denoising [35]. Wavelet transformation is advantageous for detecting weak signals by handling both time and frequency domains [36]. The Daubechies series is practical for mechanical fault detection as it is similar to impulse signals.

Large and small motors show different current waveform characteristics even in the same fault state, necessitating the development of scale-free fault detection methods. Previous studies have proposed signal preprocessing and normalization methods to address these issues. However, existing approaches still show limitations in being optimized for specific capacities or operating conditions. Therefore, a new scale-free and phase-agnostic method is required to provide consistent fault detection performance regardless of motor capacity and operating conditions.

III. A NOVEL HEALTH INDICATOR FOR SCALE-FREE AND PHASE-AGNOSTIC FAULT DETECTION

This section presents a novel health indicator for detecting ISCFs, developed by integrating (1) data acquisition, (2) preprocessing, (3) phase-agnostic health indicator calculation, and (4) calibration of a scale-free feature for different PMSM capacities, as shown in Fig. 1. As the first step, three-phase stator current signals are acquired from PMSMs. Measurements are performed under steady-state conditions. The steady-state is defined as the condition where the encoder-measured difference between successive rotation speeds is less than 1% of the current speed. As the second step, Section III-A describes how to preprocess the electrical current signal. As the third step, Section III-B depicts how to modify the conventional crest factor for phase-agnostic fault detection in detail. As the last step, Section III-C presents the interpretation of the new health indicator for detecting ISCFs, namely MMCF.

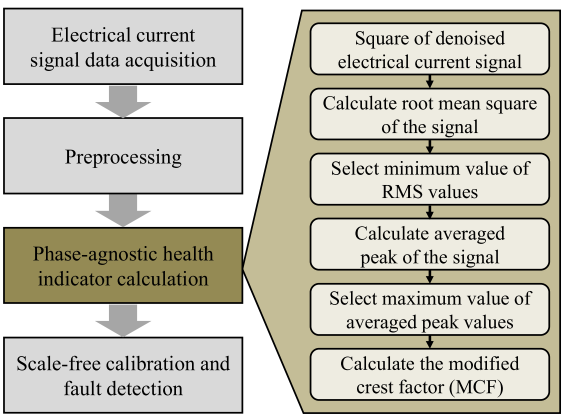

FIGURE 1. Overall procedures for detecting ISCFs.

A. PREPROCESSING

Signal preprocessing is essential to ensure the consistency of input signals used for calculating the health indicator. It directly influences both the reliability and accuracy of the resulting indicator. In this study, signal preprocessing includes zero-mean adjustment and wavelet-based denoising.

Raw current signals are measured from the three phases of the PMSM using current sensors. Although identical sensor models are employed, discrepancies may arise due to factors such as manufacturing tolerances and environmental disturbances. These variations are particularly pronounced when using low-cost sensors, which tend to exhibit greater variability in precision. As a result, the measured signals can differ across phases even under identical operating conditions. To mitigate these differences, the average value of each phase current is adjusted to zero.

The performance of wavelet denoising is highly dependent on the choice of the basis wavelet. In this study, the crest factor is employed as the selection criterion, based on the fact that an ideal sinusoidal wave exhibits a crest factor of 1.414. Accordingly, if noise is completely eliminated, the crest factor of the denoised signal should converge to 1.414. When the three-phase current of a PMSM follows a sinusoidal waveform under healthy operating conditions, this property is applicable to the measured signals. Among various candidate wavelets, the basis that yields a crest factor closest to 1.414 for the denoised healthy signal is selected.

B. MODIFIED CREST FACTOR

Regardless of motor capacity, PMSMs operate on the same principle. The three-phase current signal of a PMSM is sinusoidal. If ISCFs occur, the current signal becomes distorted by odd harmonic frequencies introduced by the fault. This study calculates the degree of distortion using the crest factor. Unlike conventional approaches that implement crest factor analysis on individual phases, the proposed method integrates information from all three phases simultaneously.

The MCF is developed to mitigate the influence of noise in the electrical current signal. The key innovation lies in replacing the conventional single peak value with an 'averaged peak' concept. This approach fundamentally differs from existing crest factor-based methods by enhancing noise immunity while preserving sensitivity to fault-induced signal distortions. As described earlier, various sources of noise are superimposed on the measured signal, distorting its shape and impairing the accuracy of fault detection. The conventional crest factor is particularly sensitive to noise, as it relies solely on the signal's peak value. Moreover, due to signal uncertainties, the crest factor may produce inconsistent results even under identical operating conditions.

The averaged peak replaces the single peak value to enhance robustness against noise. This approach is motivated by the fact that conventional denoising techniques cannot completely eliminate noise and inherent uncertainties. The averaged peak (AP) is the mean of all signal values exceeding the RMS level. Mathematically, AP(i) is defined as the mean of the $F(i)$

$$\mathrm{AP}\,(i) = \frac{1}{M} \sum F(i_k) \tag{1}$$

where i is the vector of the electrical current data measured from a PMSM, i.e., $i_1, i_2, \ldots, i_{n-1}$, and i_n. $F(i)$ is the function that filters the electrical current data i to produce a vector of elements larger than the RMS of i but smaller than the maximum value of i. M represents the number of elements in the filtered vector $F(i)$.

As illustrated in Fig. 2, the averaged peak lies between the RMS and the maximum value in a sinusoidal waveform.

One key advantage of this approach is its reduced sensitivity to random fluctuations. Since the mean of Gaussian noise is zero, its effect is inherently diminished when calculating the averaged peak. Fig. 3 shows the results of calculating both the peak value and the averaged peak value for a sinusoidal wave with an amplitude of 10, combined with noise of mean zero and standard deviation one. When this experiment is repeated under the same conditions, the peak values fluctuate with a wide distribution, whereas the averaged peak value remains relatively uniform with a narrow distribution. Therefore, AP can effectively minimize the effect of noise.

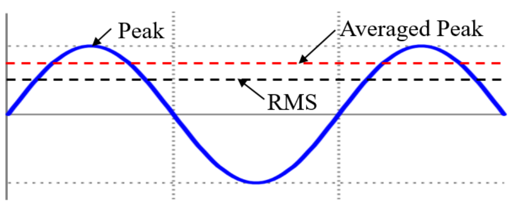

FIGURE 2. Comparisons of peak, averaged peak, and RMS values.

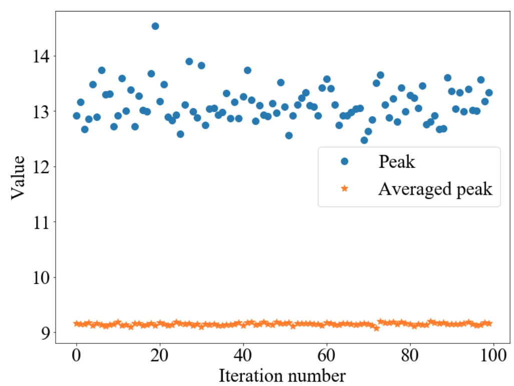

FIGURE 3. Comparisons of peak and averaged peak values.

Early detection of ISCFs is critical, as such faults can rapidly evolve into more severe conditions. However, early-stage detection is inherently challenging due to the relatively low amplitude of fault-related components in the measured signals. To address this, the proposed health indicator is specifically designed to amplify the influence of fault signatures. In particular, the square of the denoised current signal is employed in the health indicator calculation to enhance sensitivity to subtle fault effects. This squared transformation increases the relative contribution of the fault-induced deviations while suppressing residual noise, thereby improving the detectability of incipient ISCFs.

A direct comparison of maximum power levels is feasible between healthy and faulty conditions since the square of the current is proportional to the instantaneous electric power. In this study, the fault signal is artificially generated by superimposing harmonic components—specifically, a 3× sine wave with an amplitude of 0.5, a 5× sine wave with an amplitude of 0.3, and a 7× sine wave with an amplitude of 0.1—onto a fundamental 1× sine wave with an amplitude of 10.

Table 1 summarizes the amplitudes of each harmonic component in both the original and squared signals. The ratio of each harmonic to the fundamental component is also presented. While the amplitude of the generated signal decreases with increasing harmonic order, squaring the signal amplifies the relative contribution of higher-order harmonics. As a result, using the squared signal enhances the influence of subtle fault-induced components, thereby improving fault detectability.

TABLE 1. Amplitude of harmonic frequencies.

Data type	Harmonic frequency 1×	3×	5×	7×
Raw signal	9.989 (100 %)	0.990 (9.91 %)	0.487 (4.88 %)	0.091 (0.91 %)
Squared signal	39.163 (100 %)	4.573 (11.68 %)	2.312 (5.90 %)	2.338 (5.97 %)

PMSMs commonly employ three-phase windings in the stator. Due to structural and measurement-related uncertainties, the characteristics of the three windings are not perfectly identical. For example, slight differences in resistance and inductance can exist among the phases, even if they are nominally designed to be the same. As a result, the conventional crest factor yields different values for each phase, even under identical operating conditions. This inconsistency is further exacerbated when an ISCF occurs, as the fault not only affects the faulty phase but also induces disturbances in the remaining healthy phases. Consequently, calculating individual crest factors for each phase can lead to ambiguous or inconsistent results. To mitigate this issue, a single crest factor is computed using all three-phase current signals collectively, providing a unified and more reliable health indicator. The MCF is defined as the ratio of the largest averaged peak value among the three-phase current signals to the smallest root mean square (RMS) value among them.

$$\mathrm{MCF}(i_a, i_b, i_c) = \frac{\max[\mathrm{AP}(i_a^2),\ \mathrm{AP}(i_b^2),\ \mathrm{AP}(i_c^2)]}{\min[\mathrm{RMS}(i_a^2),\ \mathrm{RMS}(i_b^2),\ \mathrm{RMS}(i_c^2)]} \quad (2)$$

where i_a, i_b, and i_c are the electrical current signals measured from the three phases of PMSM.

C. PROPOSED HEALTH INDICATOR

The ideal sinusoidal waveform yields a value of 1.408 when evaluated using the proposed health indicator defined in the previous section. Since the averaged peak is used in place of a single peak, this value is lower than that of the conventional crest factor (i.e., 1.414). For more intuitive interpretation, a baseline value of 1.408 is subtracted from the calculated indicator. After calibration, a value closer to zero indicates the absence of an ISCF. However, in practical applications, the influence of noise varies between small- and large-capacity PMSMs, as the signal characteristics inherently depend on motor capacity.

The MCF computed from current signals differs across PMSMs with varying capacities, even under healthy operating conditions. To eliminate the capacity-dependent differences beyond the theoretical baseline adjustment, a calibration procedure is implemented. This procedure uses the health indicator value calculated from the current signals in the actual healthy state of each motor. The resulting value, obtained using the equation defined in the previous section, is referred to as the bias component. By subtracting this motor-specific bias from the raw health indicator, the calibrated indicator is aligned across different motor capacities. Consequently, the proposed health indicator converges to zero in the absence of ISCFs, regardless of motor capacity.

$$\mathrm{MMCF}(i_\mathrm{a}, i_\mathrm{b}, i_\mathrm{c}) = \mathrm{MCF}(i_\mathrm{a}, i_\mathrm{b}, i_\mathrm{c}) - \mathrm{MCF}(i_{\mathrm{ah},} i_{\mathrm{bh},} i_{\mathrm{ch}}) \quad (3)$$

where i_{ah}, i_{bh}, and i_{ch} are the ideal sinusoidal current waveforms, i.e., 1.408.

IV. CASE STUDIES

This section presents three case studies to validate the proposed MMCF health indicator. Section IV-A evaluates it through numerical simulations. Section IV-B describes laboratory-scale testbeds employing small-capacity PMSMs (100 W and 1 kW) with artificially induced faults. Section IV-C presents a full-scale testbed using an 82.5 kW PMSM under realistic operating conditions.

A. CASE STUDY 1: NUMERICAL SIMULATION

Acquiring signals from faulty PMSMs of different capacities by experimentation is both costly and time-consuming. In particular, applying various fault severities to PMSMs of different capacities is extremely difficult. In this study, electrical current signals were obtained from PMSMs of different capacities via an ISCF simulation. Details on the fault simulation can be found in [29]. The simulation was performed using MATLAB/Simulink. Under the nominal torque and rotation speed conditions, the current signals were recorded once the steady state defined by Eq. (4) was satisfied.

$$|v(k) - v(k-1)| \leq 0.01 \times v(k) \quad (4)$$

where v is the rotation speed of PMSM measured at the k^{th} state.

Table 2 summarizes the parameters of PMSMs used in the simulation. PMSMs with the rated capacities of 100 W and 1.1 kW were selected. The signals were acquired while varying the fault severity from the healthy state to a 5% ISCF state.

The performance of three established fault detection methods was compared in Fig. 4: (a) EPVA [15], (b) FFT-based harmonic analysis [29], and (c) Negative-sequence component method [28]. The results demonstrate significant capacity-dependent variations in all three conventional methods. The EPVA method shows 45.2% average capacity variation due to trajectory patterns scaling with motor capacity, while the FFT-based harmonic analysis exhibits 39.7% average variation due to different harmonic characteristics between 4-pole and 8-pole motor designs. Most notably, the negative-sequence component method shows relatively higher variability with 134.1% average variation due to its reliance on absolute current values, presenting a challenge for capacity-independent fault detection applications.

TABLE 2. Parameters of the PMSM for simulation.

Parameters	1st PMSM	2nd PMSM	Unit
Rated power	1100	100	W
Rated torque	3.1	0.318	N·m
Rated speed	3000	3000	r
Stator resistance	1.6	7.5	Ω
Synchronous inductance	0.006	0.009	H
Number of pole	8	4	-
Flux linkage	0.0568	0.0568	Wb
Rotor inertia	5.00×10^{-3}	2.26×10^{-5}	$\mathrm{kg\cdot m^2}$

Fig. 5 presents the result of applying the proposed MMCF health indicator to the signals measured from the fault simulation. The correlation coefficient between the proposed health indicator and fault severity is one, indicating a perfect positive correlation. Notably, the MMCF health indicator demonstrates superior scale-free characteristics with only 34.8% average capacity variation compared to existing methods. To further validate the effectiveness of the indicator, quantitative evaluation was performed using two established prognostic metrics: monotonicity and trendability [37], as detailed in Table 3. Monotonicity, which reflects the consistency of the indicator's progression as fault severity increases, yielded a value of 1.0. Trendability, which quantifies the similarity of this progression across motors with different capacities, also resulted in a value of 1.0. These results confirm that the proposed MMCF health indicator not only tracks fault development reliably, but also ensures consistent performance regardless of motor capacity.

TABLE 3. Health indicator performance comparison.

Method	Monotonicity	Trendability	Fitness
Max-mix crest factor (Proposed)	1.00	1.00	2.00
Extended Park's vector approach	0.90	0.90	1.80
FFT-based harmonic analysis	0.80	0.85	1.65
Negative-sequence component method	1.00	0.88	1.88

B. CASE STUDY 2: TESTBED WITH ARTIFICIAL FAULT SEEDING

In this case study, the proposed health indicator is evaluated using signals from a PMSM with an artificially introduced fault. A testbed was designed to measure electrical current data in the healthy and faulty states of PMSMs of different capacities, as shown in Fig. 6.

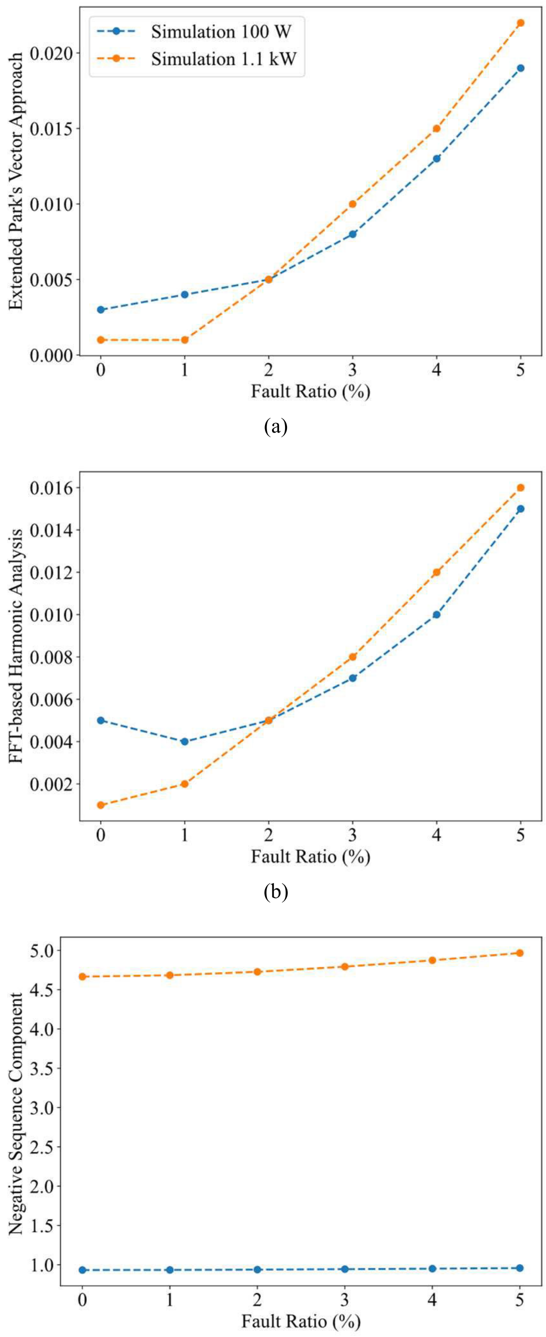

(a)

(b)

(c)

FIGURE 4. Comparative performance of existing methods under ISCF for 100 W and 1.1 kW: (a) Extended Park's vector approach [15], (b) FFT-based harmonic analysis [29], and (c) Negative-sequence component method [28].

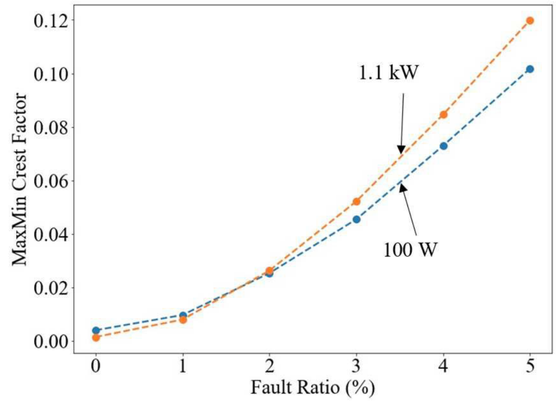

FIGURE 5. The proposed max–min crest factor computed from simulations under ISCF.

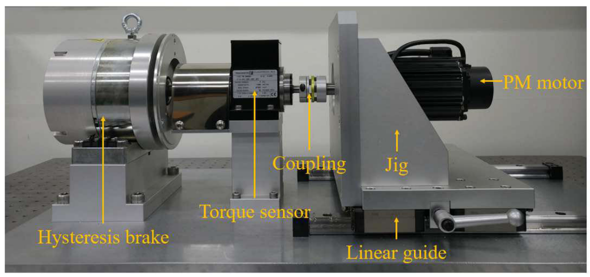

FIGURE 6. Testbed for PMSMs with different power capacities.

(a) (b)

FIGURE 7. Stator winding with ISCF: (a) 100 W and (b) 1 kW.

TABLE 4. Specifications of the PMSM used in the experiment.

Parameters	CN01	CN10	Unit
Rated power	100	1000	W
Rated torque	0.32	3.18	N·m
Rated speed	3000	3000	RPM
Rated current	0.90	5.80	A
Weight	0.55	3.7	kg
Maintenance history	New product	New product	-

The testbed includes a hysteresis brake, a torque sensor, a coupling, and a linear guide. The BHB-3BA hysteresis brake applies a load to PMSM, whereas the torque sensor (model TM306) measures torque. Flexible couplings and a linear guide were used to prevent misalignment faults. The different capacity motors used in the experiment are summarized in Table 4.

Both motors have the same manufacturer and operating conditions but different capacities. ISCFs were artificially seeded into PMSMs to acquire fault data. After disassembling PMSM, the fault was introduced by connecting an additional circuit between turns using the same type of wire as the winding. Fig. 7 shows the faulty windings of the 100 W and 1 kW PMSMs.

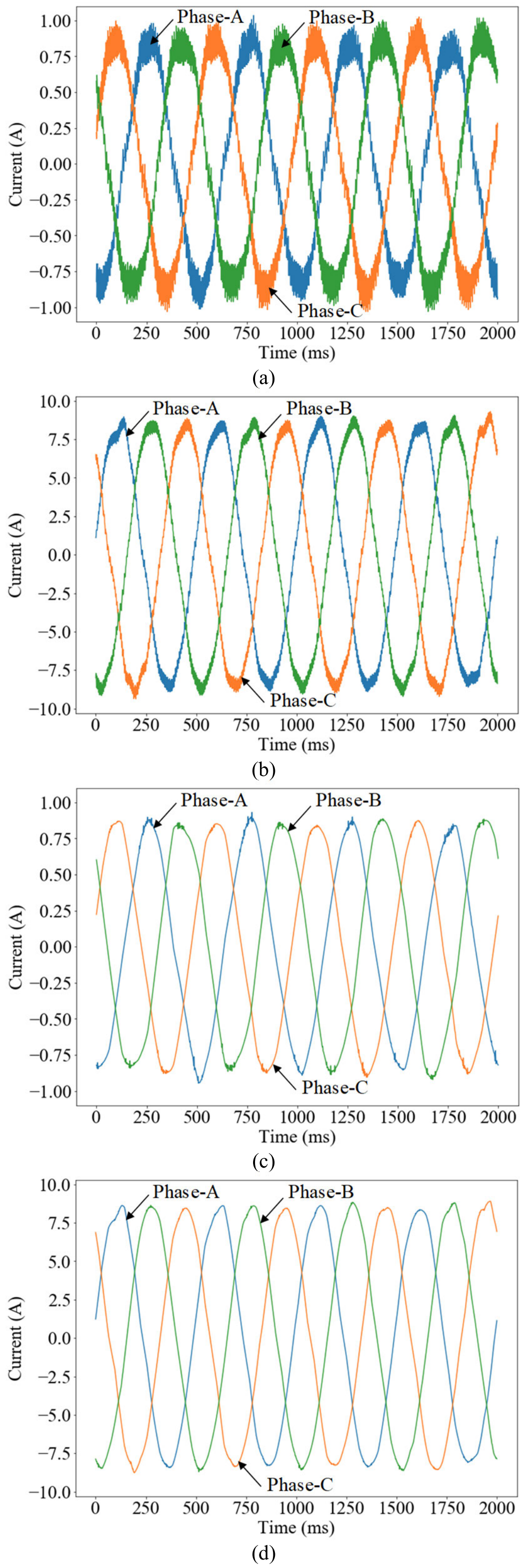

FIGURE 8. Electrical current signals of a healthy PMSM: (a) raw signal from a 100 W PMSM, (b) raw signal from a 1 kW PMSM, (c) denoised signal from a 100 W PMSM, and (d) denoised signal from a 1 kW PMSM.

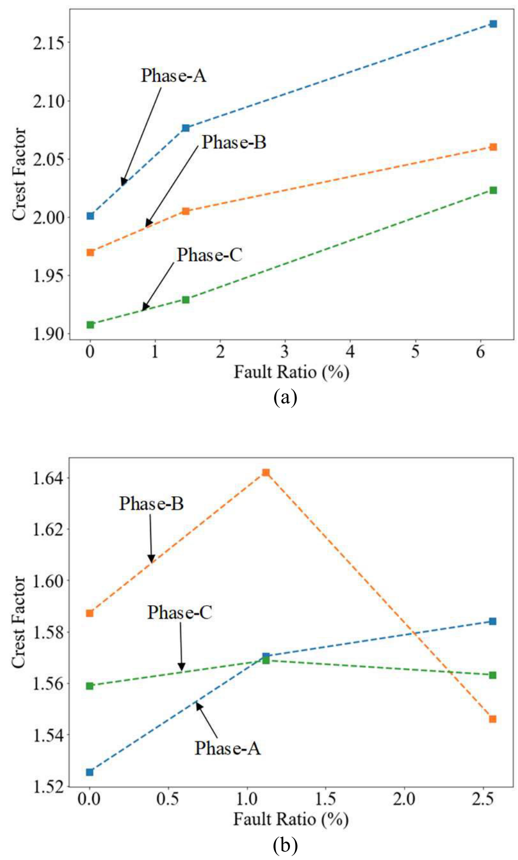

FIGURE 9. Crest factor computed from experiments under ISCF: (a) 100 W and (b) 1 kW.

Table 5 summarizes the changes in stator winding resistance resulting from fault seeding. The current signal was measured from the artificially fault-seeded PMSM at a rated load and rated rotation speed for one second at a sampling rate of 100 kHz.

TABLE 5. Results of artificial fault seeding tests.

State	100 W PMSM	1 kW PMSM
Per phase resistance	11.20 Ω (100 %)	450 mΩ (100 %)
Short fault resistance #1	165 mΩ (1.47 %)	5.04 mΩ (1.12 %)
Short fault resistance #2	659 mΩ (6.20 %)	11.54 mΩ (2.56 %)

Fig. 8 shows the raw and denoised current signals measured in the healthy state. The basis wavelet used for preprocessing was ‘rbio5.5’, selected based on the crest factor. A comparison of the signals before and after preprocessing confirmed that the noise was significantly reduced.

The conventional crest factor was calculated using the current signal measured from the testbed. As shown in Fig. 9, the crest factor tends to increase with fault severity in the faulty phase but not in other phases. In the case of the 100 W motor, the crest factor was calculated to be larger than that of a pure sine wave despite being in the healthy state. Fault detection is unreliable because the crest factor is calculated differently for the two motors.

Fig. 10 presents the results of applying the proposed health indicator to the signal measured from the testbed. The results were obtained through signal preprocessing, health indicator calculation, and the calibration process. Regardless of PMSM's capacity, the proposed health indicator increases linearly with fault severity. Moreover, the proposed health indicator and fault severity exhibit a perfect positive correlation. It is corroborated that the proposed health indicator effectively detects interturn short-circuit faults regardless of motor capacity.

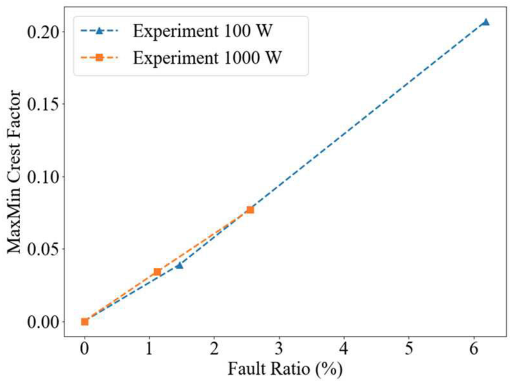

FIGURE 10. The proposed max-min crest factor is computed from experiments under ISCF.

C. CASE STUDY 3: REAL APPLICATION

In this case study, the proposed health indicator was implemented on a PMSM in a centrifugal pump to assess the health state of the stator winding. Centrifugal pumps are typical infrastructure equipment in manufacturing process systems (e.g., the refining industry). Monitoring the pump's health state in real time through the proposed health indicator can improve reliability and reduce maintenance costs. PMSM, as shown in Fig. 11, is an essential component of the centrifugal pump, making fault detection crucial.

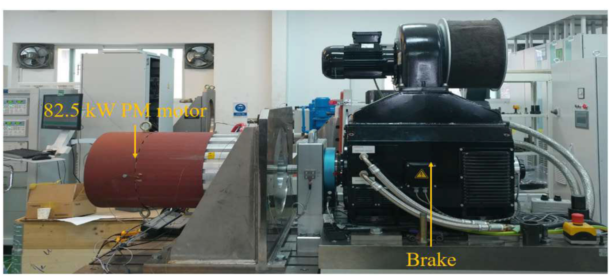

FIGURE 11. PMSM mounted on a centrifugal pump.

A current signal was measured from an 82.5 kW PMSM at the rated speed and load. Fig. 12 shows the raw and denoised current signals after preprocessing. Through visual inspection, it is confirmed that noise was effectively reduced during preprocessing.

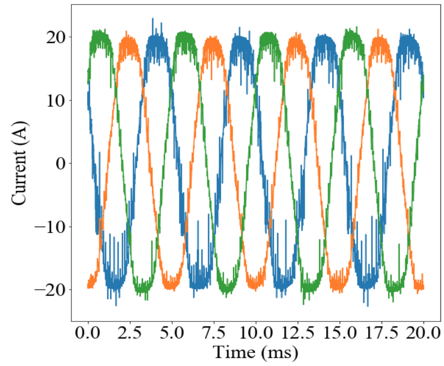

(a)

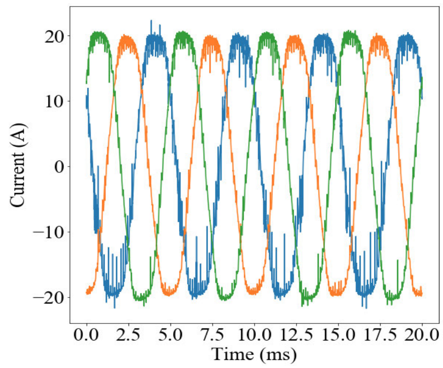

(b)

FIGURE 12. Current signals of an 82.5 kW PMSM in a healthy state: (a) raw signal and (b) denoised signal.

The result of calculating the proposed health indicator using the measured signal is shown in Fig. 13. Since the motor used for measurement is a new and healthy product, the proposed health indicator value is zero. Therefore, it can be confirmed that the indicator functions properly in PMSMs used in real applications.

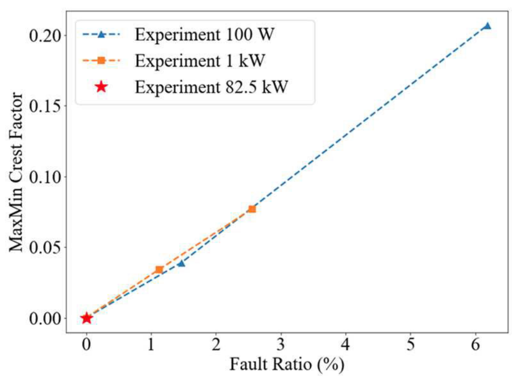

FIGURE 13. The proposed max–min crest factor for real-world application.

V. CONCLUSION

This study has presented a scale-free and phase-agnostic method for detecting ISCFs in PMSMs. The proposed method was validated through three progressive case studies across motors of different capacities. In simulation-based evaluations, the proposed MMCF health indicator exhibited a strong linear correlation with fault severity. While conventional crest factor values varied inconsistently with motor size, MMCF maintained a consistent baseline of 1.408 for ideal sinusoidal waveforms, enabling reliable and interpretable fault detection. In testbed-based validations with 100 W and 1.1 kW PMSMs, the results were consistent across different motor capacities. Furthermore, in a field application involving an 82.5 kW PMSM installed in a centrifugal pump, the proposed method yielded a zero value in the healthy state, verifying its effectiveness in practical scenarios.

The contribution of this work lies in developing a scale-free and phase-agnostic fault detection method that leverages waveform-invariant characteristics of stator current signals. The proposed method enhances fault detection performance through three integrated techniques: (1) introduction of an averaged peak concept that replaces conventional single peak values to enhance noise immunity while preserving fault sensitivity, (2) implementation of signal squaring techniques that amplify subtle fault-induced harmonic components for early-stage detection, and (3) development of a scale-free calibration methodology that eliminates motor capacity dependencies without requiring motor-specific parameters. The proposed approach requires only current measurements, supporting non-intrusive implementation without additional sensors or motor-specific parameters. These characteristics make the method well-suited for industrial applications where motors of various sizes are deployed, offering potential benefits in reducing maintenance costs and improving system reliability.

Future research should examine the proposed health indicator under various operating conditions beyond the steady-state scenarios tested in this study, including transient states and dynamic loading conditions. Particular attention should be given to evaluating the baseline calibration robustness under dynamic load variations, potentially requiring adaptive calibration strategies for real-time industrial applications. Additional testing with broader industrial environments, including high-harmonic applications and various inverter types, would further validate the method's robustness beyond the sinusoidal waveform assumption. Future work may explore phase-specific fault localization capabilities to further enhance the practical fault detection utility of the proposed method.

ACKNOWLEDGMENT

(Mikyung Hwang and Jonghyeok Kim contributed equally to this work.)

REFERENCES

[1] H. Wang, J. Wang, X. Wang, S. Lu, C. Hu, and W. Cao, "Detection and evaluation of the interturn short circuit fault in a BLDC-based hub motor," *IEEE Trans. Ind. Electron.*, vol. 70, no. 3, pp. 3055–3068, Mar. 2023, doi: 10.1109/TIE.2022.3167167.

[2] M. Y. Metwly, C. L. Clark, J. He, and B. Xie, "A review of robotic arm joint motors and online health monitoring techniques," *IEEE Access*, vol. 12, pp. 128791–128809, 2024, doi: 10.1109/ACCESS.2024.3447573.

[3] H. Saavedra, J.-C. Urresty, J.-R. Riba, and L. Romeral, "Detection of interturn faults in PMSMs with different winding configurations," *Energy Convers. Manage.*, vol. 79, pp. 534–542, Mar. 2014, doi: 10.1016/j.enconman.2013.12.059.

[4] H. Wang, J. Hu, and Y. Li, "Interturn fault severity monitoring in symmetrical six-phase PMSMs using subspace negative-sequence high-frequency current residuals," *IEEE Trans. Power Electron.*, vol. 39, no. 3, pp. 3613–3622, Mar. 2024, doi: 10.1109/TPEL.2023.3347662.

[5] Y. Zhu, S. Cai, and B. Li, "Detection and discrimination of interturn fault and high-resistance connection fault in PMSM based on deviation angle of zero sequence voltage," *IEEE Trans. Transport. Electrific.*, vol. 10, no. 3, pp. 7623–7632, Sep. 2024, doi: 10.1109/TTE.2023.3344711.

[6] Y. Qin, G. J. Li, Z. Q. Zhu, M. P. Foster, D. A. Stone, C. J. Jia, and P. McKeever, "Model-based Luenberger state observer for detecting interturn short circuits in PM machines," *IEEE Trans. Transport. Electrific.*, vol. 11, no. 2, pp. 5302–5311, Apr. 2025, doi: 10.1109/tte.2024.3478840.

[7] W. Huang, B. Du, T. Li, Y. Sun, Y. Cheng, and S. Cui, "Inter-turn short-circuit fault diagnosis of interior permanent magnet synchronous motor for electric vehicle based on search coil," *IEEE Trans. Power Electron.*, vol. 38, no. 2, pp. 2506–2515, Feb. 2023, doi: 10.1109/TPEL.2022.3213512.

[8] Y. Qi, E. Bostanci, M. Zafarani, and B. Akin, "Severity estimation of interturn short circuit fault for PMSM," *IEEE Trans. Ind. Electron.*, vol. 66, no. 9, pp. 7260–7269, Sep. 2019, doi: 10.1109/TIE.2018.2879281.

[9] M. Choi, C. Lee, S. Park, M. Hwang, and H. Oh, "Frequency-enhanced network with self-supervised learning for anomaly detection of hydraulic piston pumps," *Expert Syst. Appl.*, vol. 282, Jul. 2025, Art. no. 127662, doi: 10.1016/j.eswa.2025.127662.

[10] J. Oh, D. Yoo, C. Kim, H. Oh, Y. Ryu, K.-W. Lee, and D.-U. Sung, "A hybrid fault diagnostic approach using operational transfer path analysis and denoising deep learning with remote sensors: Application to electric vehicles," *Expert Syst. Appl.*, vol. 270, Apr. 2025, Art. no. 126470, doi: 10.1016/j.eswa.2025.126470.

[11] X. Wu, M. Li, Y. Geng, and H. Qian, "Unsupervised diagnosis of interturn short circuit of permanent magnet synchronous motor guided by density-based clustering and deep learning," *IEEE Trans. Instrum. Meas.*, vol. 74, pp. 1–11, 2025, doi: 10.1109/TIM.2024.3522658.

[12] Y. Li, R. Wang, R. Mao, Y. Zhang, K. Zhu, Y. Li, and J. Zhang, "A fault diagnosis method based on an improved deep Q-network for the interturn short circuits of a permanent magnet synchronous motor," *IEEE Trans. Transport. Electrific.*, vol. 10, no. 2, pp. 3870–3887, Jun. 2024, doi: 10.1109/TTE.2023.3306437.

[13] Z. Xu, J. Zhang, Y. Zhang, and J. Zhao, "Winding condition monitoring for inverter-fed PMSM using high-frequency current injection," *IEEE Trans. Ind. Appl.*, vol. 57, no. 6, pp. 5818–5828, Nov. 2021, doi: 10.1109/TIA.2021.3103923.

[14] R. Hu, J. Wang, A. R. Mills, E. Chong, and Z. Sun, "Current-residual-based stator interturn fault detection in permanent magnet machines," *IEEE Trans. Ind. Electron.*, vol. 68, no. 1, pp. 59–69, Jan. 2021, doi: 10.1109/TIE.2020.2965500.

[15] S. M. A. Cruz and A. J. M. Cardoso, "Stator winding fault diagnosis in three-phase synchronous and asynchronous motors, by the extended Park's vector approach," *IEEE Trans. Ind. Appl.*, vol. 37, no. 5, pp. 1227–1233, Sep. 2001, doi: 10.1109/28.952496.

[16] Y. Wu, J. Zhang, Z. Xu, S. Wang, and H. Fu, "Feature extraction and applicability comparisons for fault detection of inter-turn short-circuited PMSM," *IEEE Trans. Instrum. Meas.*, vol. 73, pp. 1–10, 2024, doi: 10.1109/TIM.2024.3415792.

[17] M. Sumislawska, K. N. Gyftakis, D. F. Kavanagh, M. D. McCulloch, K. J. Burnham, and D. A. Howey, "The impact of thermal degradation on properties of electrical machine winding insulation material," *IEEE Trans. Ind. Appl.*, vol. 52, no. 4, pp. 2951–2960, Jul. 2016, doi: 10.1109/TIA.2016.2544745.

[18] D. Niu and D. Song, "Model-based robust fault diagnosis of incipient ITSC for PMSM in elevator traction system," *IEEE Trans. Instrum. Meas.*, vol. 72, pp. 1–12, 2023, doi: 10.1109/TIM.2023.3318696.

[19] M. Li, Y. Geng, W. Wang, M. Tu, and X. Wu, "Permanent magnet synchronous motor inter-turn short circuit diagnosis based on physical-data dual model under oil-drilling environment," *Eng. Appl. Artif. Intell.*, vol. 132, Jun. 2024, Art. no. 107938, doi: 10.1016/j.engappai.2024.107938.

[20] Z. Xu, C. Hu, F. Yang, S.-H. Kuo, C.-K. Goh, A. Gupta, and S. Nadarajan, "Data-driven inter-turn short circuit fault detection in induction machines," *IEEE Access*, vol. 5, pp. 25055–25068, 2017, doi: 10.1109/ACCESS.2017.2764474.

[21] Y. Li, Y. Wang, Y. Zhang, and J. Zhang, "Diagnosis of inter-turn short circuit of permanent magnet synchronous motor based on deep learning and small fault samples," *Neurocomputing*, vol. 442, pp. 348–358, Jun. 2021, doi: 10.1016/j.neucom.2020.04.160.

[22] D. Lee, J. G. Lee, M. Choi, C. Park, C. W. Kim, G. Niu, and H. Oh, "Multi-fidelity sub-label-guided transfer network with physically interpretable synthetic datasets for rotor fault diagnosis," *Eng. Appl. Artif. Intell.*, vol. 148, May 2025, Art. no. 110467, doi: 10.1016/j.engappai.2025.110467.

[23] D. Yoo, M. Choi, H. Oh, and B. Han, "A simple but effective way to handle rotating machine fault diagnosis with imbalanced-class data: Repetitive learning using an advanced domain adaptation model," *IEEE Access*, vol. 12, pp. 189789–189803, 2024, doi: 10.1109/ACCESS.2024.3516525.

[24] Y. Hu, S. Cheng, J. Hu, W. Huang, X. Li, and Q. Sun, "Motor interturn short-circuit fault detection using leakage current," *IEEE Trans. Instrum. Meas.*, vol. 74, pp. 1–10, 2025, doi: 10.1109/TIM.2024.3509588.

[25] Q. Song, M. Wang, W. Lai, and S. Zhao, "On Bayesian optimization-based residual CNN for estimation of inter-turn short circuit fault in PMSM," *IEEE Trans. Power Electron.*, vol. 38, no. 2, pp. 2456–2468, Feb. 2023, doi: 10.1109/TPEL.2022.3207181.

[26] G. Niu, X. Dong, and Y. Chen, "Motor fault diagnostics (don't short) based on current signatures: A review," *IEEE Trans. Instrum. Meas.*, vol. 72, pp. 1–19, 2023, doi: 10.1109/TIM.2023.3285999.

[27] F. Parvin, J. Faiz, Y. Qi, A. Kalhor, and B. Akin, "A comprehensive interturn fault severity diagnosis method for permanent magnet synchronous motors based on transformer neural networks," *IEEE Trans. Ind. Informat.*, vol. 19, no. 11, pp. 10923–10933, Nov. 2023, doi: 10.1109/TII.2023.3242773.

[28] H. Jeong, S. Moon, and S. W. Kim, "An early stage interturn fault diagnosis of PMSMs by using negative-sequence components," *IEEE Trans. Ind. Electron.*, vol. 64, no. 7, pp. 5701–5708, Jul. 2017, doi: 10.1109/TIE.2017.2677355.

[29] L. Romeral, J. C. Urresty, J.-R. R. Ruiz, and A. G. Espinosa, "Modeling of surface-mounted permanent magnet synchronous motors with stator winding interturn faults," *IEEE Trans. Ind. Electron.*, vol. 58, no. 5, pp. 1576–1585, May 2011, doi: 10.1109/TIE.2010.2062480.

[30] S. Zhao, Y. Chen, F. Liang, S. Zhang, N. Shahbaz, S. Wang, Y. Zhao, W. Deng, and Y. Cheng, "Identifying early stator fault severity in DFIGs based on adaptive feature mode decomposition and multiscale complex component current trajectories," *IEEE Trans. Instrum. Meas.*, vol. 73, pp. 1–16, 2024, doi: 10.1109/TIM.2024.3443347.

[31] J. Yuan, Z. Song, H. Jiang, Q. Zhao, Q. Zeng, and Y. Wei, "The Msegram: A useful multichannel feature synchronous extraction tool for detecting rolling bearing faults," *Mech. Syst. Signal Process.*, vol. 187, Mar. 2023, Art. no. 109923, doi: 10.1016/j.ymssp.2022.109923.

[32] A. R. Bastami and S. Vahid, "A comprehensive evaluation of the effect of defect size in rolling element bearings on the statistical features of the vibration signal," *Mech. Syst. Signal Process.*, vol. 151, Apr. 2021, Art. no. 107334, doi: 10.1016/j.ymssp.2020.107334.

[33] Y. Yang, W. Xia, J. Han, Y. Song, J. Wang, and Y. Dai, "Vibration analysis for tooth crack detection in a spur gear system with clearance nonlinearity," *Int. J. Mech. Sci.*, vols. 157–158, pp. 648–661, Jul. 2019, doi: 10.1016/j.ijmecsci.2019.05.012.

[34] J. Hang, X. Shu, S. Ding, and Y. Huang, "Robust open-circuit fault diagnosis for PMSM drives using wavelet convolutional neural network with small samples of normalized current vector trajectory graph," *IEEE Trans. Ind. Electron.*, vol. 70, no. 8, pp. 7653–7663, Aug. 2023, doi: 10.1109/TIE.2022.3231304.

[35] M. Li, S. Yang, J. He, X. Gu, Y. Xu, F. Gu, and A. D. Ball, "Full-field extraction of subtle displacement components via phase-projection wavelet denoising for vision-based vibration measurement," *Mech. Syst. Signal Process.*, vol. 224, Feb. 2025, Art. no. 112021, doi: 10.1016/j.ymssp.2024.112021.

[36] S. G. Mallat, "A theory for multiresolution signal decomposition: The wavelet representation," *IEEE Trans. Pattern Anal. Mach. Intell.*, vol. 11, no. 7, pp. 674–693, Jul. 1989, doi: 10.1109/34.192463.

[37] J. Coble and J. W. Hines, "Identifying optimal prognostic parameters from data: A genetic algorithms approach," in *Proc. Annu. Conf. Prognostics Health Manag. Soc.*, Jan. 2009, vol. 1, no. 1, pp. 1–11.

MIKYUNG HWANG received the B.S. degree in mechatronics engineering from Korea University of Technology and Education, Chungcheongnam-do, Republic of Korea, in 2012, and the M.S. degree in mechatronics engineering from Gwangju Institute of Science and Technology, Gwangju, Republic of Korea, in 2014, where she is currently pursuing the Ph.D. degree in mechanical and robotics engineering. Her current research interest includes prognostics and health management for electric motors.

JONGHYEOK KIM received the B.S. degree in civil and environmental engineering from Hanbat National University, Daejeon, Republic of Korea, in 2024. He is currently pursuing the M.S. degree in mechanical and robotics engineering with Gwangju Institute of Science and Technology, Gwangju, Republic of Korea. His current research interest includes prognostics and health management for electric motors.

HYUNTAK LEE received the B.S. degree in mechanical engineering from Seoul National University of Science and Technology, Seoul, Republic of Korea, in 2017, and the M.S. degree in mechanical engineering from Gwangju Institute of Science and Technology, Gwangju, Republic of Korea, in 2019. His current research interest includes prognostics and health management for electric motors.

HYUNSEOK OH received the B.S. degree in mechanical engineering from Korea University, Seoul, Republic of Korea, in 2004, the M.S. degree in mechanical engineering from Korea Advanced Institute of Science and Technology, Daejeon, Republic of Korea, in 2006, and the Ph.D. degree in mechanical engineering from the University of Maryland, College Park, MD, USA, in 2012. He is currently an Associate Professor with the Department of the Mechanical and Robotics Engineering, Gwangju Institute of Science and Technology, Gwangju, Republic of Korea. His research interests include fault diagnostics, industrial artificial intelligence, and physics-informed neural networks.